Indirect measurements of neutron-induced reaction cross sections at storage rings

B. Jurado, M. Sguazzin, J. Pibernat, P. Alfaurt, T. Chiron, M. Roche, B. Thomas, T. Kurtukian, I. Tsekhanovich
Centre d'Etudes Nucléaires de Bordeaux-Gradignan (CENBG), France

J. Glorius, Y. A. Litvinov, C. Brandau, A. Gumberidze, S. Hagmann, P.-M. Hillenbrand, A. Kalinin, M. Lestinsky, S. Litvinov, B. Lorentz, E. Menz, N. Petridis, U. Popp, M.S. Sanjari, U. Spillmann, M. Steck, Th. Stöhlker
GSI Helmholtzzentrum für Schwerionenforschung, Darmstadt, Germany

M. Grieser, K. Blaum
Max-Planck-Institut für Kernphysik, Heidelberg, Germany

R. Reifarth, K. Göbel
Goethe Universität Frankfurt, Frankfurt am Main, Germany

V. Méot, M. Dupuis, A. Chatillon, L. Gaudefroy, O. Roig, J. Taïeb
CEA, DAM, DIF, France

C. Bruno, T. Davinson, C. Lederer-Woods, J. Marsh, P. J. Woods
The University of Edinburgh, Edinburgh, United Kingdom

A. Henriques
FRIB/NSCL, Michigan State University, USA

Ch. Langer
FH Aachen, 52428 Aachen, Germany

L. Audouin, F. Hammache
Irene Joliot Curie LAB, Orsay, France

W. Korten, L. Thulliez
CEA Paris-Saclay - DRF/IRFU/DPhN, France

A. Heinz
Chalmers University of Technology, Gothenburg, Sweden

C. Domingo Pardo
Instituto de Física Corpuscular, CSIC-Universidad de Valencia, Spain

Y. Zhang
Institute of Modern Physics, Lanzhou, China

T. Yamaguchi
University of Saitama, Saitama, Japan

H. Fynbo
Aarhus Universitet, Aarhus, Denmark

Spokesperson: Beatriz Jurado, CENBG, France

Abstract: Obtaining reliable cross sections for neutron-induced reactions on unstable nuclei is a highly important task and a major challenge. These data are essential for understanding the synthesis of heavy elements in stars and for applications in nuclear technology. However, their measurement is very complicated as both projectile and target are radioactive. The best alternative to infer these cross sections is to use the surrogate-reaction method in inverse kinematics, where the nucleus formed in the neutron-induced reaction of interest is produced by a reaction involving a radioactive

heavy-ion beam and a stable, light target nucleus. The decay probabilities (for fission, neutron and γ-ray emission) of the nucleus produced by the surrogate reaction provide precious information to constrain models and enable much more accurate predictions of the desired neutron cross sections.

We propose to investigate surrogate reactions in inverse kinematics at the CRYRING@ESR, which is the ideal instrument for this purpose as it will allow us to measure the decay probabilities of many short-lived nuclei with unrivaled accuracy. The first step in the development of our new methodology at the CRYRING@ESR is a proof-of-principle experiment at the ESR. In this first experiment, we will apply our new technique to infer the γ- and neutron-emission probabilities of ^{208}Pb. The excited ^{208}Pb nucleus will be formed by the inelastic scattering ^{208}Pb(p,p') surrogate reaction at an incident energy of 30 AMeV. The measured probabilities will be used to validate our new method and to improve the predictions for the ^{207}Pb(n,γ) and ^{207}Pb(n,n') reaction cross sections, which are relevant for the design of lead-cooled fast reactors and for nuclear astrophysics.

This proposal is part of the ERC-Advanced grant NECTAR (Nuclear rEaCTions At storage Rings), PI: B. Jurado.

Collaboration: SPARC

1. INTRODUCTION

1.1. Motivation

Most of the elements from iron to uranium are synthesized in stars via neutron-induced reactions during the slow (*s*) and rapid (*r*) neutron-capture processes. The r-process is terminated at extremely neutron-rich nuclei in the actinide region undergoing fission. Fission recycling can then occur where the produced fission fragments continue to undergo neutron captures and β decays until fission again terminates the r-process path. After a few cycles, the abundances in the mass region $120 < A < 210$ can become dominated by the fission-fragment distributions.

However, the s- and r-processes cannot explain all the observed elemental abundances. Some observations may be explained by the intermediate neutron-capture process (the i-process), which has regained significant attraction in the last years [1]. The reaction flow of the i-process path occurs two to six mass numbers away from stability and its understanding is hampered by the uncertainty in the neutron capture cross sections of unstable nuclei along the i-process path, see e.g. [2, 3].

The r-process requires explosive stellar scenarios. The recent detection of gravitational waves from the merger of two neutron stars [4], and the subsequent kilonova, consistent with being powered by the radioactive decay of nuclei synthesized by the r-process [5, 6], demonstrated that neutron-star mergers are an important r-process site. Still, many uncertainties and open questions remain regarding the r-process. For instance, it is not yet clear if the r-process abundance distribution in the solar system is the result of one or multiple scenarios. The measurement of neutron-induced cross sections of key neutron-rich nuclei is essential to answer this question [7]. Sensitivity studies on neutron radiative capture cross sections described in [8] show that the key nuclei are concentrated near closed shells and in the rare-earth region, where they impact the formation of the rare-earth peak of the r-process abundance pattern. Many of the open questions on the r-process are related to the role of nuclear fission, since we do not know whether fission recycling occurs and how fission influences r-process observables such as abundance patterns and light curves. Key physical quantities for understanding the impact of fission are neutron-induced fission cross sections, fission-barrier properties and fission-fragment yields [9, 10, 7]. It is difficult to predict the range of fissioning nuclei of interest since this significantly depends on the fission barriers, for which models give very different predictions. According to [9, 11], the nuclei that play a major role are located near the N = 184 shell closure with Z≈90-98. However, in [10] the key fissioning nuclei are not only located near N = 184 but also at N < 184, because, according to their models, fission is still very active during the decay back to stability. Fission barriers have also a dramatic impact on spontaneous fission half-lives, a modification of the fission barrier of typically 1 MeV can affect the half-life up to 9 orders of magnitude. These half-lives determine if spontaneous fission powers the late-time-kilonovae light curves, for example in [12] the potential importance of spontaneous fission heating was pointed out.

Neutron-induced cross sections of radioactive nuclei are also crucial ingredients for the simulation of advanced nuclear systems for the transmutation of nuclear waste or for the development of innovative fuel cycles like the thorium cycle [13]. The nuclei of interest for transmutation are Np and Am isotopes, whereas for the thorium cycle the key nuclei are located near ^{232}Th and ^{233}U. For many of these nuclei the existing data are of very limited quality [14]. Even for the fission cross sections there are often large uncertainties and important discrepancies between different sets of data [15].

1.2. Neutron-induced reactions

A neutron-induced reaction at incident energies below a few MeV can be mainly described as a two-step process (Fig. 1). In the first step, the nucleus A will absorb the neutron forming a compound nucleus (A+1)*. The excited compound nucleus can then decay in different ways: (a) by emitting γ-rays, this is the radiative neutron capture reaction (n,γ). (b) By emitting a neutron, leaving the nucleus mass A and proton Z numbers unchanged, this is denoted elastic (n,n) or inelastic scattering (n,n'). (c) By fission, (n,f), if the compound nucleus is heavy enough. Each decay mode has a given probability (P_γ, P_n, P_f) and the sum of the probabilities of all the possible decay channels must be 1.

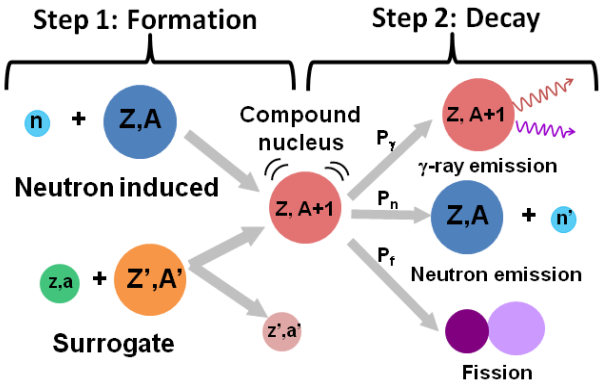

***Figure 1**: Sequence of a neutron-induced reaction. First a compound nucleus is formed, which then de-excites by the emission of γ-rays, a neutron or by fission. The probability P associated to each decay channel is indicated. In a surrogate reaction, the same compound nucleus as in the neutron-induced reaction is produced by a different reaction.*

In traditional neutron-irradiation experiments, the direct measurement of neutron-induced cross sections of short-lived nuclei is very challenging: (a) the production and handling of radioactive targets is very complicated due to radiation-protection requirements. (b) The radioactivity of the target creates a background very difficult to distinguish from the signals coming from the decay of nucleus (A+1)* and can severely damage the detectors. (c) Often, the strong background from scattered beam neutrons in the target, the set-up and the surroundings strongly impairs the measurements, even on stable nuclei.

When the target nuclei are radioactive, most of the neutron-induced cross sections rely on theoretical model predictions. However, these predictions often yield huge uncertainties due to the difficulties in describing the compound-nucleus de-excitation process (step 2 in Fig. 1). Indeed, the de-excitation process is ruled by fundamental properties (level densities, fission barriers, transmission coefficients, etc.) for which the existing nuclear models give very different predictions. This leads to discrepancies between the calculated cross sections as large as two orders of magnitude or more when no experimental data are available [16, 17].

1.3. Surrogate reactions

The difficulties associated with the measurement of neutron-induced cross sections of radioactive nuclei cannot be overcome by performing the measurements in inverse kinematics at radioactive ion beam facilities since free neutron targets are not available. The best alternative to infer these cross sections is to use the surrogate-reaction method in inverse kinematics. The surrogate reaction produces the compound nucleus of interest by a different reaction than the neutron-induced reaction (compare Fig. 1) and the decay probabilities for fission, γ and neutron emission are measured as a function of the excitation energy of the compound nucleus. The measured decay probabilities are used to constrain model parameters (fission barriers, particle transmission coefficients, level densities, etc.) and enable much more accurate predictions of the desired neutron cross sections. Of particular interest is the (d,p) surrogate reaction, where a heavy-ion beam is directed onto a deuterium gas target. During the reaction, the neutron of the deuterium target is transferred to the projectile nucleus. The (d,p) reaction thus appears intuitively as the closest reaction to a neutron-induced reaction in inverse kinematics.

An interesting aspect of surrogate reactions is that several reactions can be investigated simultaneously with a single projectile-target combination. For instance, in an experiment involving a heavy projectile A and a D_2 deuterium target, it will also be possible to investigate the inelastic-scattering of deuterons (d,d') and the (d,t) reaction, which produce two different compound systems. An additional advantage of surrogate reactions is that with one incident beam energy it is possible to populate a broad excitation-energy distribution of the compound nucleus (from 0 to about 15 MeV). Thus, it is possible to measure the decay probabilities of different nuclei as a function of excitation energy in one experiment.

To infer the decay probabilities in inverse kinematics we need to: (a) identify the different target-like residues (i.e. distinguish between protons, deuterons and tritons). (b) Precisely know the energy of the beam and the target-like residues, as well as the emission angle of the target-like nuclei with respect to the beam. This will allow us to calculate the excitation energy of the compound nucleus by applying energy and linear-momentum conservation. (c) Detect the products of the compound-nucleus decay in coincidence with target-like residues.

1.3.1. Previous studies

Fission probabilities induced by nuclear transfer and inelastic-scattering reactions represent the most direct observable to infer fission barriers and are also a unique tool to study the level structure and the level density in the vicinity of the fission barrier, see e.g. [18]. Another particularly interesting aspect of fission probabilities is that they can be used to infer neutron-induced fission cross sections by applying the "Weisskopf-Ewing" (WE) approximation. Within the WE approximation, which is valid at sufficiently high excitation energies, the decay of a compound nucleus is considered to be independent of its spin J and parity π; i.e., it is assumed that the decay probabilities of the compound nucleus are identical for the neutron-induced and the surrogate reactions [19]. In this case, the desired neutron cross section can be obtained applying the equation:

$$\sigma_{n,\chi}(E_n) = \sigma_n^{CN}(E_n) \cdot P_\chi(E^*) \quad (1)$$

where $\sigma_n^{CN}(E_n)$ is the cross section for the formation of a compound nucleus after the absorption of a neutron of incident energy E_n, E* is the excitation energy of the compound nucleus and P_χ is the probability that the compound nucleus formed by the surrogate reaction decays via channel χ. E_n and E* are related via $E_n=(E^*-S_n)\cdot(A+1)/(A)$, where S_n is the neutron separation energy of the compound nucleus. The compound-nucleus formation cross section σ_n^{CN} is calculated with optical potentials and has an uncertainty of less than 10% for nuclei not very far from stability [19]. The factorization of the cross section in eq. (1) into the product of the formation cross section and the decay probability reflects the independence of the formation and the decay steps inherent to the formation of a compound nucleus, which is a nucleus in statistical equilibrium.

A number of experiments involving actinides not far from ^{238}U performed in direct kinematics by our collaboration, e.g. [20], and by other groups in the USA [19] showed that the fission cross sections derived using eq. (1) are in very good agreement with directly measured neutron-induced fission cross sections. This is particularly useful since the theoretical predictions for the fission probabilities are quite uncertain due to the lack of knowledge on the level structure in the vicinity of the fission barrier. In addition, to infer the fission probabilities one has also to model the competition with all the other open decay channels. This requires an accurate knowledge of the nuclear structure properties of the nuclei involved in the decay, which is available to some extent only near the stability valley where experimental data exist.

However, the WE approximation fails when applied to infer neutron-induced fission cross sections of even-even fissioning nuclei [21]. This has been attributed to the spin-parity mismatch, i.e. the differences between the angular momenta and parity populated in the neutron-induced and surrogate reactions, and the very low density of states on top of the fission barrier of even-even nuclei, which leads to a significant dependence of the fission probability on J^π.

Furthermore, a group at the Lawrence Livermore National Laboratory in the USA [22] and our collaboration [23] observed that the radiative-capture cross sections of rare-earth nuclei obtained with eq. (1) were up to a factor 10 larger than the directly-measured neutron-induced cross sections. This is also explained by the J^{π} mismatch. Indeed, at excitation energies close to the neutron separation energy S_n, neutron emission is very sensitive to the spin of the decaying nucleus (A+1)*, because only the ground state and the first excited states of the residual nucleus A formed after neutron emission can be populated. When the angular momentum of (A+1)* is much larger than the angular momentum of the first states of nucleus A, neutron emission is hindered and the excited nucleus (A+1)* mainly decays by γ emission, which is the only open decay channel [23].

When the WE approximation fails, a different strategy is needed. This strategy consists in predicting the J^{π} distributions populated in the surrogate reaction and combining them with the decay probabilities obtained with the surrogate reaction to fix the values of the parameters of some of the key ingredients of the statistical model like fission barriers, neutron transmission coefficients, level densities and γ-ray strength functions. With the newly-tuned parameters the model gives an accurate prediction of the desired neutron cross section. This strategy has recently been proven for radiative neutron capture in two benchmark experiments where the emission probabilities for selected γ-ray transitions were measured. In [24], the ^{92}Zr(p,d) reaction was used to infer the well-known ^{90}Zr(n,γ) cross section, and in [25] the ^{95}Mo(d,p) reaction was used to infer the ^{95}Mo(n,γ) cross section.

Very recently, we have made an important step forward and applied this new strategy to infer both the neutron-induced fission and radiative capture cross sections of ^{239}Pu [26]. This was achieved by combining simultaneously-measured fission and γ-emission probabilities for the ^{240}Pu(^{4}He, ^{4}He')^{240}Pu* surrogate reaction with a calculation of the J^{π} distributions populated in this reaction. We stress an additional significant improvement with respect to [24] and [25], namely that, instead of measuring the probabilities for a few selected γ-ray transitions, we measured the γ-emission probability, i.e. the probability that the compound nucleus releases its entire E* by emitting a cascade of γ rays. This leads to a more precise determination of the model parameters since it does not require modelling all the details of the γ-ray cascade. For instance, the latter modelling has to include the branching ratios of all the low-lying transitions, which are often unknown. With our data we were able to determine the first fission-barrier height of the even-even ^{240}Pu nucleus with an uncertainty of only 20 keV, much lower than the typical uncertainty of fission barriers of 100-200 keV. The relative uncertainties of the resulting neutron-induced cross sections of ^{239}Pu vary between 5 and 20%, depending on the neutron energy [26].

We propose to infer neutron-induced cross sections of nuclei of interest in nuclear astrophysics and applications by simultaneously measuring the decay probabilities of all the open decay channels (fission, γ and neutron emission). In this way, we will be able to define with much better precision the set of parameters that describes the full de-excitation process. Moreover, measuring the decay probabilities for all the open decay channels provides also a strong test to the experimental technique, because the sum of the probabilities must be equal to 1 [26]. It will also be very useful to measure in the same experiment the angular distributions of the target-like products, since they will strongly constrain the models used to predict the J^{π} distribution of the surrogate reaction [24].

1.3.2. Need for surrogate-reaction studies in inverse kinematics

The proposed measurements cannot be performed in direct kinematics for several reasons: (a) Very often, the nuclei of interest are highly radioactive and the necessary targets are unavailable. (b) Competing reactions in target contaminants and backings produce a high background that is very complicated or even impossible to remove, see e.g. [18]. (c) The heavy products of the decay of the compound nucleus are stopped in the target sample and cannot be detected. Therefore, the measurement of γ- and neutron-emission probabilities requires detecting the emitted γ rays and neutrons, which is rather difficult due to the very low detection efficiencies [27].

The limitations (a) and (c) can be overcome in inverse kinematics. This requires a high areal density of target atoms. However, the different isotopes of H and He, as the most promising candidates for

surrogates, are gases. High areal densities of these materials are very difficult to achieve and cause several problems: (a) Pressurized gas cells and cryogenic targets require entrance and exit windows. The beam can interact with the window material generating a strong background. (b) Chemical compounds like CH_2 have the same disadvantages as windows. (c) Windowless gas or cryogenic targets with high areal densities are large. This results in a very limited resolution of the interaction point. (d) The resolution of the emission angle of the target-like residue relative to the direction of the incoming projectile is reduced if the nuclei straggle in the target material before and after the reaction. (e) The projectile ions and reaction products lose energy due to the interaction with the electrons of the thick target.

The emission angle and the energy of the target-like residue as well as the projectile energy are therefore uncertain, which significantly limits the resolution in the excitation energy of the compound nucleus. The decay probabilities change very rapidly with excitation energy at S_n and at the fission threshold. The excitation-energy resolution required to scan this rapid evolution is a few 100 keV, quite difficult to achieve for heavy nuclei in inverse kinematics [28].

1.4. The advantages of heavy-ion storage rings

We propose to address the discussed limitations by investigating for the first time surrogate reactions at the CRYRING@ESR [29] storage-ring complex of GSI/FAIR, which offers unique possibilities for the study of nuclear reactions.

A key capability of storage rings is beam cooling, which allows for a significant reduction of the size and energy spread of the stored beam induced by the reaction mechanism used to produce it or by the interaction with internal targets. Beam cooling takes typically a few seconds and ensures an extraordinary quality of the stored beam in terms of emittance and momentum spread. If a gas target is present in the ring, the electron cooler can compensate the energy loss as well as the energy and angular straggling of the beam in the gas target. Hence, the ions pass the target always with the same energy and the same outstanding quality, quite in contrast to single-pass experiments. Moreover, the frequent passing of the target zone (about 1 million times per second at 10 AMeV) allows ultra-thin gas targets (10^{13} atoms/cm^2) to be used and no windows are necessary. This is a great improvement for surrogate reactions since the beam will only interact with the desired material and in a well-defined interaction zone, while the luminosity remains on a high level.

The ESR can be used to reduce the energy of the stored beam from a few 100 AMeV, the typical energy required to produce bare ions, to a few AMeV. This enables another unique feature: the production of 10 AMeV cooled beams of fully-stripped radioactive heavy ions. In addition, since the gas target has a very low density, the probability for electron capture reactions before or after the nuclear reaction is extremely low. Therefore, the beam-like residues produced by the nuclear reaction will also be fully striped. This is also very useful for our measurements, as discussed in section 2.1. All these advantages are only possible with storage rings. They enable the determination of the excitation energy and the decay probabilities of the compound nucleus with unrivalled accuracy.

GSI/FAIR is the only facility worldwide where two heavy-ion storage rings are connected together (CRYRING@ESR). The ESR is used to slow down and cool the beam that is then injected into the CRYRING, where the measurements are performed while the ESR prepares the next ion bunch. In this way, no time is lost in the preparation of the beam. Beam cooling and deceleration takes about a minute, which sets the lower limit of the half-life of the radioactive ions that can be prepared.

Heavy-ion storage rings are operated in ultra-high vacuum (UHV) conditions (10^{-10} to 10^{-12} mbar), which poses severe constraints to in-ring detection systems. UHV-compatible silicon detectors have started to be used only recently for the study of nuclear reactions at the ESR [30, 31].

2. MEDIUM AND LONG-TERM PLAN: SURROGATE-REACTION STUDIES AT ESR@CRYRING

Our ultimate goal is to simultaneously measure the fission, γ- and neutron-emission probabilities induced by transfer and inelastic scattering reactions at CRYRING@ESR, and to use the measured

decay probabilities to indirectly infer the neutron cross sections of many short-lived nuclides in different regions of the chart of nuclei. For example, using beams of ^{237,238}Np, ^{233,234,235,236,237,238}U, $^{230, 231, 232}$Th we will be able to investigate the region around ^{238}U, which is highly relevant for nuclear-reactor physics. It will also be possible to explore the region of neutron-deficient actinides and pre-actinides near the N=126 shell closure. These studies will help to provide much better predictions for the fission barriers and cross sections near the shell closure N=184, which are essential for the r-process [9, 10, 11] and not yet accessible to experiments. We can also investigate lighter nuclei of great relevance for the i-process. For instance, we can use the ^{135}I(d,p) surrogate reaction to infer the ^{135}I(n,γ) cross section, which is one of the most important data [32], but is very difficult to measure due to the short half-life of ^{135}I of about 6 h.

We would like to start our program of measurements at CRYRING@ESR by conducting an experiment with a $^{238}U^{92+}$ beam at 11 AMeV on a deuterium gas-jet target. The kinematics of two-body reactions involving a heavy projectile (e.g. ^{238}U) at about 10 AMeV and a light target (^{2}H) leads to target-like residues covering a broad range of angles from 0 to 180°, whereas the associated projectile-like residues are very much forward focused with maximum emission angles of less than 0.5°. The fission fragments are emitted within a cone of about 20°. The required set-up to perform the measurement is presented in the upper part of Fig. 2.

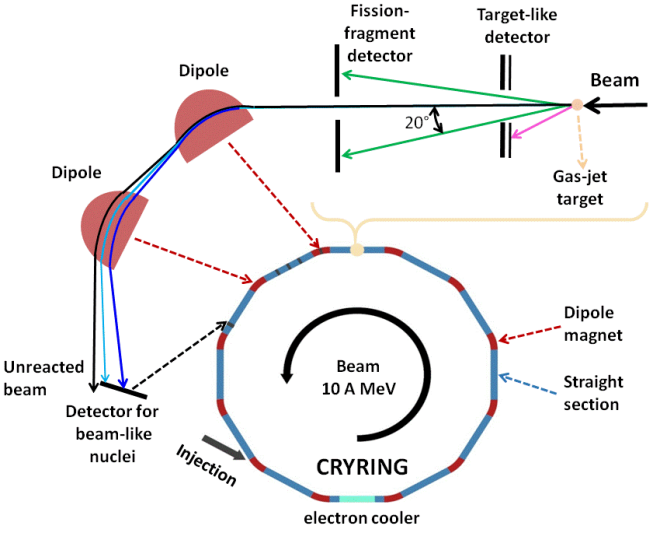

Figure 2: *The lower part shows a schematic view of the CRYRING. The upper part shows a schematic view of the experimental setup that will be placed inside the CRYRING for the simultaneous measurement of fission, γ- and neutron-emission probabilities. The trajectories of the heavy beam-like residues produced after γ and neutron emission are shown in light blue and blue, respectively.*

It consists of: (a) a particle telescope ΔE-E to identify and measure the kinetic energies and angles of the target-like nuclei. (b) A fission detector covering forward angles to detect fission fragments in coincidence with target-like nuclei. (c) A detector for measuring the number of heavy beam-like products formed after γ-ray or neutron emission, detected in coincidence with target-like nuclei. The beam-like detector is placed after the second dipole magnet downstream from the reaction zone. The dipoles will separate the beam and the different beam-like residues according to their magnetic rigidity. The decay probabilities as a function of the excitation energy E* are given by:

$$P_{\chi}(E^*) = \frac{N_{c,\chi}(E^*)}{N_{tl}(E^*)\cdot\varepsilon_{\chi}(E^*)} \qquad (2)$$

where N_{tl} is the number of target-like nuclei detected, $N_{c,\chi}$ is the number of coincidences measured between the residues of decay channel χ and the target-like nuclei, and ε_{χ} is the efficiency for detecting the residues of decay channel χ.

To avoid the UHV constraints, detectors are often placed inside a pocket and separated from the UHV by a thin stainless-steel window of typically 25 μm. In our experiment, the fission-fragment kinetic energies can be as low as 5 AMeV. These fragments are stopped in the stainless-steel window. Therefore, the fission-fragment detectors have to be directly placed in UHV. This is very challenging and we propose a completely new solution, which is to build these detectors with solar cells, the devices that are routinely used to convert the sunlight into electricity. We have shown recently that solar cells have good energy and time resolution when used to detect heavy ions at ~ 10 AMeV [33]. In addition, they are extremely affordable (about 5 Euros!) and much more resistant to radiation damage than the traditionally-used silicon detectors [34]. Their radiation hardness is of great

advantage for in-ring measurements, since replacing damaged detectors implies venting the reaction chamber and re-establishing UHV, even in a small part of the ring, can take several days or even weeks.

As in the proton-capture experiments [31], our set-up will be completed with high-purity germanium detectors surrounding the target (not shown in Fig. 2). They will be used to detect the x-ray signature of the radiative electron capture process. The cross sections for this process can be predicted with an uncertainty ≤ 2% and are very well suited for determining the luminosity in the ring. With this information, it will be possible to determine the cross sections as a function of angle of the target-like nuclei, which, as said above, are very useful for predicting the populated J^{π} distributions. Note that the decay probabilities P_{χ} will be measured at different emission angles of the target-like residues. Their comparison will allow us to investigate the impact of the compound nucleus spin and parity on the decay probabilities, since the populated J^{π} distribution depends on the emission angle.

2.1. Expected performances

We have performed very detailed Geant4 simulations for the inelastic ^{238}U(d,d') scattering reaction, where we have tracked all the reaction residues from the target until the different detectors.

We have considered a thin, position-sensitive ΔE detector (128x48 mm^2, 128 horizontal and 48 vertical strips). Thanks to the ultra-low density target and the electron cooling, it is possible to neglect the energy loss and the straggling of the beam and the scattered target-like residues in the target. We have considered the straggling of the scattered target-like residues in the stainless-steel window of the pocket. The effect of the latter on the excitation-energy resolution is negligible. In addition, we have included a radius of the gas-jet target of 0.5 mm, a beam momentum spread $\sigma(p)/p=2\cdot10^{-4}$, a beam emittance of 0.05 mm·mrad and an energy resolution of the telescope of $\sigma(E)/E=1\%$. Considering deuteron residues emitted at 40° and an excitation energy of the ^{238}U compound nucleus of 8.2 MeV our simulations give an excitation-energy resolution $\sigma(E^*)\approx230$ keV, which is outstanding for a heavy beam as ^{238}U [28]. This value is mainly determined by the energy resolution of the telescope. If $\sigma(E)/E$ is increased to 2%, we obtain $\sigma(E^*)\approx300$ keV. With $\sigma(E)/E$=1 or 2 % and a beam emittance of 0.5 mm·mrad we have $\sigma(E^*) \approx 470$ keV.

The forward focusing of the fission fragments in inverse kinematics results in a detection efficiency for fission events as high as 96%, while in direct kinematics the fission efficiency varies between 50 and 60% [20, 27].

In direct kinematics, it is not possible to detect the heavy residues of the reaction and the γ-emission probability is measured by counting γ rays with detection efficiencies varying from 5 to 10% [23, 27]. Because of the difficulty to detect neutrons, the neutron-emission probability is generally not measured. The situation is radically different in inverse kinematics where the detection of heavy residues is possible. To determine the γ- and neutron-emission probabilities (see eq. 2) we have to discriminate between the beam-like residues A+1 and A produced after prompt-γ and prompt-neutron emission, respectively, and to evaluate the detection loses in order to infer the associated detection efficiencies. The best discrimination between the two residues is achieved at the focal point of CRYRING, which is located at the end of the straight section placed after the second dipole, see Fig. 2. The position of the residues for the ^{238}U(d,d') reaction corresponding to an excitation energy of ^{238}U* of 8.2 MeV and scattered deuterons emitted at 40° is shown in Fig. 3. The simulation includes the recoil experienced by the ^{237}U nucleus after neutron emission, which broadens the position distribution.

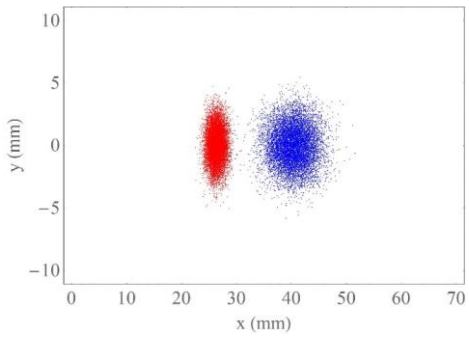

Figure 3: *Position of the residues formed after γ, $^{238}U^{92+}$(red), and neutron emission, $^{237}U^{92+}$(blue), at the focal point of the CRYRING for the ^{238}U(d,d') reaction.*

The position distributions of the two residues are very well separated from the beam nuclei (which are at x=0) and also from each other. The detectors have to be positioned at x > 10 mm to let the beam and the elastic

scattered beam-like nuclei pass through. In the case of the ^{238}U(d,d') reaction, 100% of the $^{238}U^{92+}$ residues and 97% of the $^{237}U^{92+}$ residues are transmitted to the focal point of CRYRING. This implies detection efficiencies for inferring γ and neutron-emission probabilities close to 100%, much larger than the efficiencies obtained in direct kinematics. Note that we will not have to deal with the intense background of ^{238}U beam ions produced after e^- stripping reactions in the target, since the beam ions are fully stripped. The beam ions produced after e^- capture in the target are not an issue neither, as they have a smaller charge, i.e. a larger magnetic rigidity, and are bent outside the ring, far from the γ and neutron-emission residues.

3. SHORT-TERM PLAN: PROOF-OF-PRINCIPLE EXPERIMENT AT THE ESR

The measurements described above require the development of the set-up shown in Fig. 2. This development will start in 2021 and take about 3 years, it will be done within the ERC grant NECTAR. For 2021/2022, we propose to perform a proof-of-principle experiment at the ESR to investigate two of the key points of our measurements: (a) The excitation energy, resolution and systematic uncertainties. (b) The transmission and the separation of the beam-like residues.

A $^{208}Pb^{82+}$ beam at 30 AMeV will interact with a hydrogen gas-jet target. We will consider the elastic ^{208}Pb(p,p) and the inelastic ^{208}Pb(p,p')^{208}Pb* scattering reactions. We have chosen ^{208}Pb because it is within the mass range of nuclei we are interested in and its ground state and first excited states are well separated in energy. The number of events, mean values and the widths of the peaks corresponding to the ground and excited states of ^{208}Pb in the measured E* spectrum will allow us to detect possible systematic uncertainties and determine the achieved E* resolution. Moreover, since the excitation energies of the first excited states are well known, they will be very useful to calibrate our target-like detector in energy, as we do in our experiments in direct kinematics [18]. This method of calibration will be compared with other methods consisting in changing the beam energy by 1 or 2 AMeV to shift the kinetic energy of the target-like residues or in using an alpha source. The two latter methods will be used for nuclei that do not have well separated states.

The measurement of the position and the number of detected beam-like residues will allow us to benchmark the simulations describing the trajectories of the heavy residues within the ring. These simulations require a precise knowledge of the ring parameters. We will also verify that the sum of the measured probabilities for γ and neutron emission is equal to 1, which represents a stringent test of our new methodology. Once the validation is done, we will use the measured probabilities to improve the predictions for the ^{208}Pb(n,γ) and ^{208}Pb(n,n') cross sections, which are relevant for applications and astrophysics.

Another advantage of this first experiment is that the required reaction chambers are already available, so that the measurement can be performed in 2021 or early 2022 and we can profit in due time from the acquired knowledge to optimize the design of the set-up for the CRYRING experiment. This proof-of-principle experiment will be part of the PhD Thesis of M. Sguazzin.

3.1. Experimental set-up

Fig. 4 shows the set-up of the proof of principle experiment at the ESR. The scattered protons will be detected with a telescope centered at 60° with respect to the beam axis at a distance of 8.4 cm from the gas-jet target. The telescope will be composed of a DSSSD and a stack of two Si(Li) detectors. The beam-like residues will be detected with a DSSSD placed in the detector station located downstream from the first dipole after the target section. As for the measurements at the CRYRING, this detector will be placed at least 10 mm from the beam axis. The characteristics of the detectors are given in Table 1. All the detectors will be placed inside pockets with a stainless-steel window of 25 μm.

Detector	Detector type and quantity	Size	Number of channels	Angular coverage
Target-like	ΔE: 1xDSSSD (300 μm thick)	35x35 mm^2	32+32	48 to 72°
	E: 2xSi(Li) (6 mm thick)	40x40 mm^2	2x4	
Beam-like	DSSSD (500 μm thick)	100x48 mm^2	128+48	-

Table 1: Main characteristics of the detectors for the proof of principle experiment.

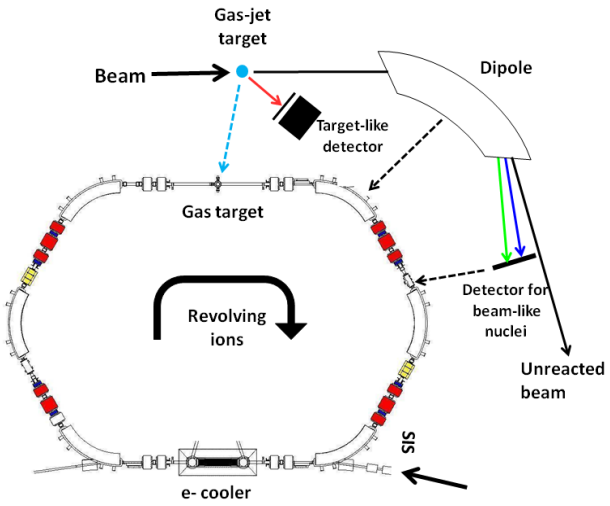

Figure 4: *The lower part shows a schematic view of the ESR. The upper part shows the setup for the proof of principle experiment. The trajectories of the heavy beam-like residues produced after emission of γ rays ($^{208}Pb^{82+}$) and a neutron ($^{207}Pb^{82+}$) are shown in blue and green, respectively.*

If we assume a beam emittance of 0.5 mm·mrad, a beam momentum spread $\sigma(p)/p=2\cdot10^{-4}$, an energy resolution of the telescope of $\sigma(E)/E=1\%$ and a target radius of 0.5 mm, our simulations give an excitation-energy resolution (standard deviation) of $\sigma(E^*)\approx300$ keV for the ground state of ^{208}Pb ($E^*=0$) and elastically scattered protons detected at 60°. The effect of the target radius on the E* resolution is very important. Indeed, if we consider a target radius of 2.5 mm we obtain $\sigma(E^*)\approx800$ keV at $E^*=0$ and $\sigma(E^*)\approx 500$ keV at $E^*= 8$ MeV and a scattering angle of 55°.

Fig. 5 shows the position of the beam-like residues at the location of the detector plane. We have considered an excitation energy of ^{208}Pb of 8 MeV (0.6 MeV above S_n) and protons scattered at 55°. According to our simulations all the residues reach the detector plane. However, by comparing Fig. 3 and Fig. 5, we see that the separation of the residues is not as good as at the CRYRING and that part of the residues produced after γ emission will be lost because they are at x<10 mm. This results in detection efficiencies lower than at the CRYRING, between 56−69% for γ-emission residues and 87−96% for neutron-emission residues.

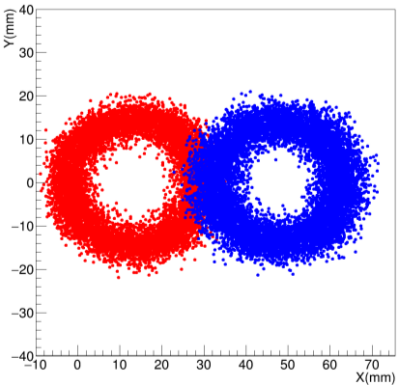

Figure 5: *Position of the residues formed after γ, $^{208}Pb^{82+}$ (red), and neutron emission, $^{207}Pb^{82+}$ (blue), at the ESR for the $^{208}Pb(p,p')$ reaction.*

3.2. Expected results and their impact

As said above, to test the developed methodology, we will verify that the measured γ-emission probability satisfies $P_\gamma=1$ below S_n and that the sum of the measured γ emission and neutron emission probabilities gives $P_\gamma+P_n=1$ above S_n.

Afterwards, we will use the measured probabilities to improve the predictions for the ^{207}Pb(n,γ) and ^{207}Pb(n,n') cross sections at neutron energies above few 100 keV. In fact, the existing evaluations suffer from the lack of data for the ^{207}Pb(n,γ) cross sections above 300 keV, whose direct measurement is very complicated due to the background resulting from neutrons scattered in the target and captured in the detectors, the cross-section ratio scatter/capture getting larger and larger with increasing neutron energy. On the other hand, the available data for the ^{207}Pb(n,n') cross section show significant discrepancies between them and with respect to the evaluated cross sections. The ^{207}Pb(n,γ) and ^{207}Pb(n,n') cross sections at neutron energies above 100 keV are important for the design of lead-cooled fast reactors. Indeed, since 22.1% of natural lead consists of ^{207}Pb these cross sections affect the neutron balance in this type of reactor systems. These cross sections are also useful to reduce the uncertainty on the values for the s-process and r-process contributions to the solar abundance of ^{207}Pb [35,36]. The use of our decay probabilities to infer neutron-induced reaction cross sections requires a reliable calculation of the J^π distribution populated in the ^{208}Pb(p,p') reaction. This calculation will be performed by M. Dupuis et al., whose microscopic model has proven to give very good results in the region of lead nuclei [37].

3.3. Beam time request

The average luminosity during a measurement cycle of duration *T* is given by:

$$\langle L \rangle = \frac{\int_{t_0}^{T} \eta L_0 e^{-\frac{t-t_0}{\tau}} dt}{T} \quad (3)$$

where ηL_0 is the luminosity at the beginning of the measurement, η is a coefficient ≤ 1 that describes the overlap between the beam and the target, τ is the lifetime of the stored ions and t_0 is the time when the measurement cycle starts. $L_0 = N_0 \cdot f \cdot N_t$, where N_0 is the number of stored $^{208}Pb^{82+}$ ions decelerated from an injection energy of 400 AMeV to the final energy, f is the revolution frequency (0.69 MHz for ^{208}Pb at 30 AMeV in the ESR) and N_t is the target areal density. The lifetime τ is determined by electron capture reactions in the gas-jet target, the e^- cooler and the residual gas. With a beam emittance of 0.5 mm·mrad, $\sigma(p)/p = 2 \cdot 10^{-4}$ and a target of 2.5 mm radius we obtain $\eta = 0.58$. This value of η and a target density $N_t = 10^{13}$ atoms/cm^2 lead to a lifetime $\tau \approx 20$ s. We estimate that t_0, the time needed to decelerate and cool the injected beam, is 20 s. Assuming T = 60 s and $N_o = 10^8$ ions, it follows that the average luminosity during one measurement cycle is $\langle L \rangle \approx 10^{26}$ cm^{-2}·s^{-1}. The different values used to obtain the average luminosity are compiled in Table 2.

Number of decelerated $^{208}Pb^{82+}$ ions N_0	Beam frequency f	H_2 target density N_t	Overlap parameter η	Lifetime τ	Preparation time t_0	Measurement time T	**Average luminosity <L>**
10^8	0.69 MHz	10^{13} atoms/cm^2	0.58	20 s	20 s	60 s	**10^{26} cm^{-2}·s^{-1}**

Table 2: *Values used to determine the average luminosity according to eq. (3).*

To determine the decay probabilities as a function of E* at a given target-like angle with a relative uncertainty of about 10%, we need to detect 10000 target-like residues within a bin of E* of ±500 keV [27]. Table 3 shows the beam time necessary to reach the required statistics at a representative E* of 8 MeV and a proton scattering angle of 55°. The cross sections have been obtained with the microscopic model of M. Dupuis et al. [37]. In case the number of decelerated, stored ions is less than 10^8, we will sum up the events over a larger angular interval around 55°.

Reaction	Telescope angle	Telescope solid angle	Cross section	Detected events	**Required beam time**
^{208}Pb(p,p') at 30 AMeV, E*=8 MeV	55±3°	0.22 sr	1.1 mb/sr	0.024 Hz	**4.8 days**

Table 3: *Values used to estimate the necessary beam time.*

The elastic scattering cross section at 55° is about 3 mb/sr. With the above luminosity, in some hours we will have several hundreds of counts in the elastic peak and sufficient statistics to perform the energy calibration at 32 AMeV.

We **request a total of 22 shifts, 6 for setting up the ESR, 1 for the energy calibration of the telescope with a beam at 32 AMeV (main users) and 15 for data taking at 30 AMeV (main users).**

4. MAJOR PUBLICATIONS OF THE SPOKESPERSON

The four most important project-related publications of the spokesperson are underlined in the list of references below.

[1] H. Schatz, J. Phys. G: Nucl. Part. Phys. **43,** 064001 (2016).
[2] M. G. Bertolli, et al. arXiv:1310.4578 (2013).
[3] P. Denissenkov et al., J. Phys. G: Nucl. Part. Phys. **45**, 055203 (2018).
[4] B. P. Abbott et al., Phys. Rev. Lett. **119**, 161101 (2017).
[5] D. M. Siegel, Eur. Phys. J. A **55**, 203 (2019).

[6] D. Watson et al., Nature **574**, 497 (2019).
[7] T. Kajino et al., Progress in Particle and Nuclear Physics **107**, 109 (2019).
[8] M. R. Mumpower et al., Progress in Particle and Nuclear Physics **86,** 86 (2016).
[9] S. Goriely, Eur. Phys. J. A **51**, 22 (2015).
[10] N. Vassh et al., J. Phys. G: Nucl. Part. Phys. **46**, 065202 (2019).
[11] M. Eichler et al., The Astrophysical Journal **808**, 30 (2015).
[12] S. Wanajo et al., Astrophys. J. **789**, L39 (2014).
[13] N. Colonna et al., Energy Environ. Sci. **3**, 1910 (2010).
[14] V. V. Zerkin and B. Pritychenko, Nucl. Instrum. Methods A 888, 31 (2018).
[15] P. Talou et al., J. Phys. G: Nucl. Part. Phys. **42,** 034025 (2015).
[16] M. Arnould and S. Goriely, Phys. Reports **384**, 1 (2003).
[17] M. Arnould et al., Phys. Reports **450**, 97 (2007).
[18] G. Kessedjian et al., Phys. Rev. C **91**, 044607 (2015).
[19] J. E. Escher et al., Rev. Mod. Phys. **84**, 353 (2012).
[20] G. Kessedjian et al., Phys Lett. B **692**, 297 (2010).
[21] W. Younes and H. C. Britt, Phys. Rev. C **67**, 024610 (2003).
[22] N. D. Scielzo et al., Phys. Rev. C **81**, 034608 (2010).
[23] G. Boutoux et al., Phys. Lett. B **712**, 319 (2012).
[24] J. E. Escher et al., Phys. Rev. Lett. **121**, 052501 (2018).
[25] A. Ratkiewicz et al., Phys. Rev. Lett. **122**, 052502 (2019).
[26] R. Pérez Sánchez et al., Submitted to Phys. Rev. Lett. (2020) http://arxiv.org/abs/2002.05439
[27] R. Pérez Sánchez et al., Nucl. Instrum. Methods A **933**, 63 (2019).
[28] W. N. Catford, The Euroschool on Exotic Beams, Vol. IV. Lecture Notes in Physics, vol **879**. Springer, Berlin, Heidelberg (2014).
[29] M. Lestinsky et al., Eur. Phys. J. Special Topics **225,** 797 (2016).
[30] J. C. Zamora et al., Phys. Rev. C **96**, 034617 (2017).
[31] J. Glorius et al., Phys Rev Lett **122**, 092701 (2019).
[32] R. Reifarth et al., J. Phys. G: Nucl. Part. Phys. **41**, 053101 (2014).
[33] A. Henriques et al., Nucl. Instrum. Methods A **969**, 163941 (2020).
[34] N.N. Ajitariand et al., Nucl. Instrum. Methods A **300**, 354 (1991).
[35] U. Ratzel et al., Phys. Rev. C **70**, 065803 (2004).
[36] C. Domingo Pardo et al., Phys. Rev. C **74**, 055802 (2006).
[37] M. Dupuis et al., Phys. Rev. C **100**, 044607 (2019).